Reaction Chemistry & Engineering

Polyolefin plastic waste hydroconversion to fuels, lubricants, and waxes: A comparative study

Journal:	*Reaction Chemistry & Engineering*
Manuscript ID	RE-PER-10-2021-000447.R1
Article Type:	Perspective
Date Submitted by the Author:	24-Nov-2021
Complete List of Authors:	Kots, Pavel; University of Delaware, Center for Plastics Innovation Vance, Brandon; University of Delaware, Chemical and Biomolecular Engineering Vlachos, Dion; University of Delaware

ARTICLE

Polyolefin plastic waste hydroconversion to fuels, lubricants, and waxes: A comparative study

Received 00th January 20xx,
Accepted 00th January 20xx

DOI: 10.1039/x0xx00000x

Pavel A. Kots [1,†], Brandon C. Vance [1,2,†], Dionisios G. Vlachos *[,1,2]

Hydroconversion technologies have surged to the forefront of deconstructing plastic waste. Recent studies have been performed over several catalysts with varying conditions and plastics that make comparisons difficult. We compile and compare data from the literature by introducing various metrics and perform a simple energy analysis. We draw mechanistic similarities to and differences from the past literature on small alkane hydroconversion and leverage the former to propose standard approaches to tune product selectivity. We exemplify the plastics materials gap and the challenges it creates. Finally, we discuss the current limitations and suggest future work.

Plastic waste (PW) represents an enormous threat due to its rapid accumulation in landfills with extensive leakage into the ecosystem[1,2]. Mechanical recycling is unsuitable to handle packaging materials, which are a major component of PW. A prime solution to this ongoing challenge relies on the development of PW chemical recycling and upcycling[3]. Polyolefins (PO), such as polyethylene (PE) and polypropylene (PP), represent more than half of all PW[3,4] and their recycling rates are the lowest. Thus, significant attention has been directed towards discovering PO conversion catalysts to transform the PW to fuel and lubricant range hydrocarbons.

[1]*Center for Plastic Innovation, University of Delaware, 221 Academy St., Newark, DE 19716, USA.*
[2]*Department of Chemical and Biomolecular Engineering, University of Delaware, 150 Academy St., Newark, DE 19716, USA.*

[†] *– equal contribution.*
[*] *- corresponding author: vlachos@udel.edu*

Electronic Supplementary Information (ESI) available: [details of any supplementary information available should be included here]. See DOI: 10.1039/x0xx00000x

Recent review articles have compiled nicely the latest advancements in PW upcycling[5–7]. Yet, an assessment of various catalysts and technologies is lacking due to significant differences in catalysts loadings, reaction conditions, and feedstocks among these studies. It is important to provide the growing PW community with comparative studies and metrics and emphasize key gaps in the PO upcycling to more efficiently direct and accelerate catalyst development. The lessons learned from the rich history of biomass and small alkane catalysis can be instrumental in this regard.

Traditional catalytic reaction engineering was focused primarily on C-C bond cracking of crude oil fractions and more recently on making new C-C bonds of building blocks of shale gas or biomass toward a higher molecular weight product. The extensive C-C bond breaking required to recycle or upcycle PO is a complicated task[6] and functionalization of the products or the feedstock may also be necessary. Future chemistry for a circular economy should partially break existing C-C bonds,[8] remake and rearrange them or noninvasively add and remove functionalities, like new C-O or C=O bonds. The biomass upcycling is an excellent example where multiple bond activations take place, including deconstruction of biopolymers to building blocks or platform molecules and selectively remaking bonds to value-added products, such as fuels, lubricants, detergents, etc.

In this comparative paper, we analyze catalytic processes from recent papers for product distribution, selectivity, productivity, and energy use and identify knowledge gaps and comparison metrics. We propose metrics and standardization procedures to accelerate learnings. We perform a simple energy analysis of various processes that indirectly provides valuable insights into CO_2 emissions. We draw mechanistic analogies to and differences from the rich small alkane chemistry and propose future directions to understand the mechanisms better. Unlike small molecule activation and biomass platform molecules, where the feedstock is molecularly known exactly, and more like the biopolymers of biomass, we exemplify the plastics materials gap and the

challenges it creates in developing technologies for actual plastic waste.

Overview of Catalytic Processes for Plastic Deconstruction

Heterogeneous catalysis offers three distinct pathways for C-C bond breaking in PO at relatively mild reaction conditions. First, hydrocracking[9] typically involves bifunctional metal/acid catalysts. It is an effective strategy to produce gasoline-range hydrocarbons from LDPE (low-density PE), HDPE (high-density PE), and PP at 225-275 °C over $Pt/WO_3/ZrO_2$ physically mixed with different solid acids. Second, monofunctional (metal) Ru- and Pt-catalysed hydrogenolysis makes heavier products, including diesel and lubricants. Metathesis coupled with dehydrogenation in excess of a low molecular weight co-reactant has also been reported.[10,11] All three routes are fundamentally distinct, which makes direct comparisons nontrivial. We refer to hydrocracking and hydrogenolysis collectively as hydroconversion. Several catalyst options were proposed for hydroconversion in the past (Table 1).[12-15] Among these catalytic technologies, metathesis is the least developed and is not discussed further.

Pyrolysis is a popular technology for converting solids. It employs high temperatures and is typically unselective and non-catalytic (a catalyst could also be invoked in the pyrolysis unit or downstream). Pyrolysis operates at higher reaction temperatures compared to hydroconversion. Under these conditions, thermal C-C bond cleavage in PO will cause their breakdown into liquid and gas products. A significant advantage of pyrolysis is its agnostic nature to the feedstock. While not the focus of this paper, we compare recent pyrolysis work to the hydroconversion catalytic technologies to provide context.

ARTICLE

Table 1. Summary of experimental hydroconversion data. MW refers to the molecular weight of the polymer. The numbers in front of an element of a catalyst (column 4) imply weight percent.

Hydrocracking											
Year	**Journal**	**Reference**	**Catalyst**	**Polymer**	**MW (kDa)**	**Polymer to catalyst ratio**	**Temperature (°C)**	**Pressure (bar)**	**Time (h)**	**Yield Liquid (%)**	**Gas Yield (%)**
1996	Energy & Fuels	Ref[12]	$0.5Pt/1.5SO_4/ZrO_2$ $0.5Pt/7WO_3/ZrO_2$ $0.5Pt/1.5SO_4/ZrO_2$	HDPE PP PP	250 250 250	5 5 5	375 325 325	83 83 83	0.42 0.33 0.33	68 72 77	35 29 23
1997	Energy & Fuels	Ref[13]	$NiMo/SiO_2$-Al_2O_3	HDPE	125	1.5	375	69	1	38	61
2011	Applied Catalysis B	Ref[14]	Ni/BETA Ni/Al-SBA-15 Ni/Al-MCM-41	LDPE	416	30	310	20	0.75 0.75 0.75	88 88 89	13 12 10
2019	Industrial and Engineering Chemistry	Ref[15]	1Pt/BEA	LDPE	150	10	330	20	0.25 0.5 1	61 43 44	39 57 56
2021	Science Advances	Ref[9]	$0.5Pt/15WO_3/ZrO_2$ + HY $0.5Pt/15WO_3/ZrO_2$ + BEA $0.5Pt/15WO_3/ZrO_2$ + HY	LDPE	76	10	250 250 275	30	2 2 1	70 41 62	30 34 19
2021	Applied Catalysis B	Ref[16]	$0.5Pt/15WO_3/ZrO_2$	LDPE	76	10	250	30	12	100	12
Hydrogenolysis											
Year	**Journal**	**Reference**	**Catalyst**	**Polymer**	**MW**	**Polymer to**	**Temperature**	**Pressure**	**Time**	**Yield**	**Gas**

					(kDa)	catalyst ratio	(°C)	(bar)	(h)	Liquid (%)	Yield (%)
2019	ACS Central Science	Ref[17]	18.8Pt/$SrTiO_3$	PE	22.15	5	300	12	24	99	N/A
2020	Science	Ref[18]	1.5Pt/γ-Al_2O_3	PE LDPE	3.5 94.5	0.59	280	1	24	70 69	9 6
2020	Nature Catalysis	Ref[19]	1.7mSiO_2/0.35Pt/SiO_2 2.4mSiO_2/0.27Pt/SiO_2 3.4mSiO_2/0.33Pt/SiO_2	HDPE HDPE HDPE	26.5 27.5 28.5	88 67 83	300 300 300	14 14 14	24 24 24	42 60 72	42 38 26
2021	JACS Au	Ref[20]	5Ru/C	PE LDPE	4 76	25 28	200 225	22 22	16 16	54 44	35 27
2021	Applied Catalysis B	Ref[21]	5Ru/CeO_2	PE LDPE	4 64 50 35	34	240	35	8 10 24 18	90 87 87 88	10 13 13 13
2021	ACS Sustainable Chemistry & Engineering	Ref[22]	5Ru/C	PP	340	14	250	40	14 16	36 25	64 73
2021	ACS Catalysis	Ref[23]	5Ru/TiO_2 5Ru/C 5Ru/CeO_2	PP	250	20	250	30	16 8 16	65.6 0 6.8	28.2 100 97.8
2021	Cell Reports Physical Science	Ref[24]	5Ru/FAU	LDPE PP	76 12	17	300	50	3 3	0 0	99 99
2021	JACS Au	Ref[25]	5Ru/15WO_3/ZrO_2 5Ru/ZrO_2 5Ru/25WO_3/ZrO_2	LDPE LDPE LDPE	76 76 76	40	250	30	2	52 60 53	23 13 8

Please do not adjust margins

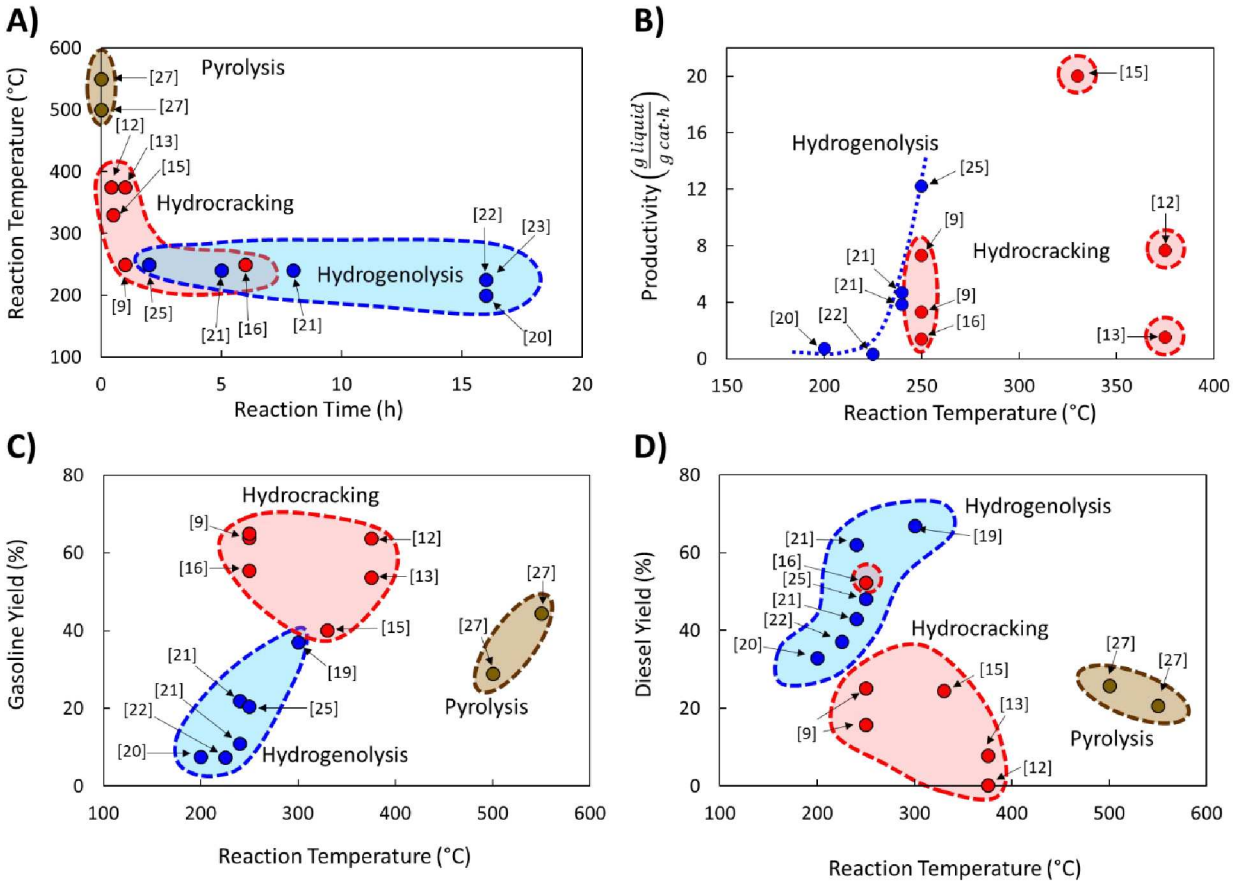

Figure 1. A) Correlation between reaction temperature and time for different PO upcycling strategies compared to pyrolysis for near complete conversion; B) Comparison of catalyst productivity to liquids with the remaining products being light gases and coke; C) Gasoline and D) diesel yields as function of reaction temperature. The brackets indicate the literature references. The colours distinguish the three processes.

Metrics and Benchmarking Catalysis

Comparing literature results is challenging because studies utilize different active phases, supports, and feedstocks (LDPE, HDPE, PP; different molecular weight; etc.). Yet, comparative studies are essential to advance the field. The significance of benchmarking in catalysis is frequently pointed out[26]. Here we discuss several benchmarking aspects and make recommendations for future work.

We compared the reaction temperatures and reaction times from several recent publications (see Table 1 for details and Fig. 1A). Compared to fast pyrolysis in a fluidized bed reactor[27], hydrocracking and hydrogenolysis operate at lower reaction temperatures and longer reaction times (Fig. 1). The lower temperatures lead to substantial energy savings discussed in the following section. Hydrogenolysis operates at lower temperatures at the expense of longer reaction times compared to hydrocracking. Nonetheless, these processes can overlap at moderate reaction conditions. The trade-off between reaction time and temperature (Fig. 1A) is expected. However, the reaction time varies significantly (by order of magnitude) depending on the catalyst, indicating the catalyst choice is vital for the CAPEX. Ru-based hydrogenolysis catalysts, especially on TiO_2[23], are very active at low temperatures. Similarly, among hydrocracking catalysts, metal/metal oxide catalysts physically mixed with zeolites operate at significantly lower temperatures than metals in zeolites and mesoporous materials, mixed metal oxides alone, or NiMo on SiO_2-Al_2O_3.

These comparisons are rather simplistic as they do not distinguish the feedstock. Table 1 exposes large variations in molecular weight and plastics among studies. Unlike small

molecule activation, the variation of the feedstock increases the complexity and makes comparisons harder. We return to this point below.

Catalyst activity should be benchmarked in turnover frequency (TOF) or turnover number (TON), which is the "numbers of turns of a catalytic cycle, equivalent to site-normalized catalytic productivities[26]". For PE and PP hydroconversion, when it is almost impossible to deduce simple reaction steps, we propose to evaluate the number of broken C-C bonds:

$$TON = \frac{\left(\sum_{reactant} N_{CC} - \sum_{products} N_{CC}\right)}{m_{cat} \cdot [site\ density]}, \frac{mol\ C-C\ bond}{mol\ of\ active\ sites}$$

Here N_{CC} is the number of C-C bonds. This calculation necessitates the estimation of metal and acid site densities using appropriate probe molecules. TONs could greatly facilitate catalyst comparisons between research groups and reveal metal-support interactions and particle size effects on reactivity.

Obviously, TON is insufficient to describe catalyst performance. C-C bonds can be broken internally (i.e., in the middle of the PE backbone[17,25]), in the terminal position leading to excessive methane formation[23], or on side chains leading to demethylation reported recently for PP hydrogenolysis over Ru/C[23]. Whenever possible, experimental TON values should be accompanied by information about the C-C bond scission location.

For example, terminal C-C bond cleavage in PE will produce light gases (mainly methane), while internal bond breaking will lead to liquids. Thus, differentiation is relatively simple. PP is more complicated, and liquid products should be characterized using NMR and/or GC. Similar to PE, terminal C^1-C^3 bond breaking will lead to methane formation. Internal C^2-C^3 bond cleavage will lead to a simple mixture of short PP oligomers (Scheme 1). In this case, liquid products will have a polypropylene-like structure with a CH_2/CH_3 molar ratio close to unity.

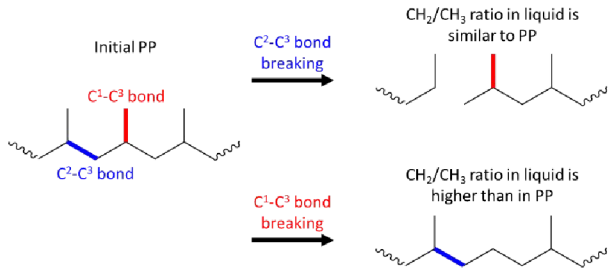

Scheme 1. Regioselectivity in C-C bond breaking of PP.

C^1-C^3 bond breaking is will remove CH_3 groups in the middle of the chain of PP (Scheme 1). This demethylation process will alter the structure of the liquid products and generate undesired methane. Accurate estimation of demethylation reactions will enable researchers to differentiate and calculate TON values for specific C-C bond cleavage types. Newly formed C^2-C^2 bonds in demethylated products can participate in secondary cracking reactions, making calculations more complicated.

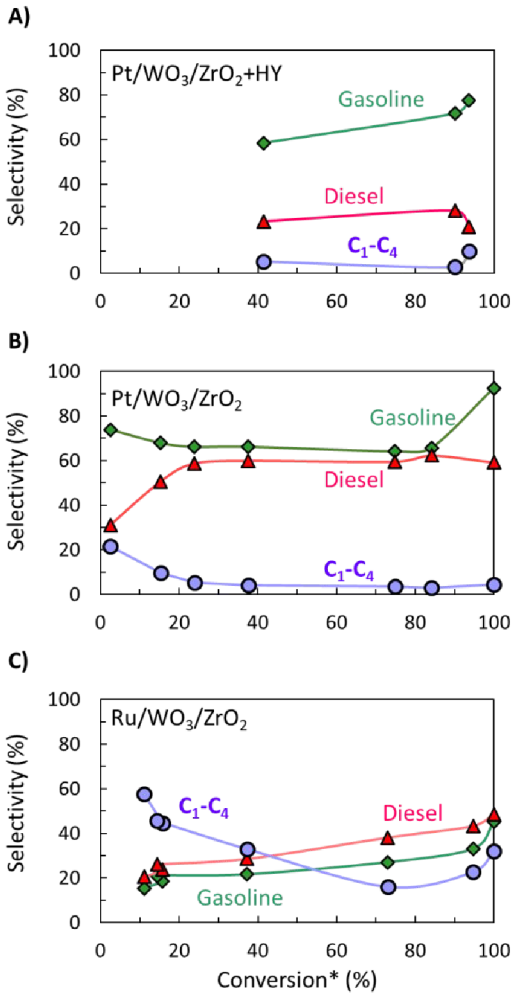

Figure 2. Selectivity to diesel, gasoline, and light gas hydrocarbons as function of apparent LDPE conversion for A) hydrocracking using a physical mixture of $Pt/WO_3/ZrO_2$ and HY[9]; B) hydrogenolysis over a pure $Pt/WO_3/ZrO_2$[16] and C) over $Ru/WO_3/ZrO_2$[25]. * - conversion was calculated based on total yield of liquid products.

Catalyst productivity should also be normalized to the total catalyst mass, not only the active component. This is important for industrial applications when the total catalyst consumption per ton of product and the productivity per m^3 of the reactor must meet strict limits[28]. For instance, the catalyst consumption per ton of liquid products from PO should be in the range of ~0.1-1 kg/ton, leading to an ideal polymer to catalyst mass ratio of 100-1000 in one reaction run. Published studies operate primarily with plastic to polymer ratios in the range of 0.5 – 30 (Table 1). More active catalysts are clearly needed.

Fig. 1B shows catalyst productivities compiled from recent papers. Those works did not aim at process optimization and productivity enhancement. Fig. 1B compares the amount of liquid produced per time and the amount of hydrocracking or hydrogenolysis catalyst. This metric accounts for the ratio of plastics to the catalyst and the reaction time that vary widely

among studies (Table 1). Furthermore, the selectivity to light gases over liquids varies among catalysts. The data shows that at very low temperatures (200-250 °C), both hydrogenolysis and hydrocracking offer similar productivity. Hydrogenolysis exposes an upper limit at ~250 °C above which extensive methane forms, leading to lower liquid yields (a volcano type of behavior). At high temperatures, hydrocracking performance is increased due predominantly to the shortening of the reaction time[9,15].

PO conversion products can be grouped into gasoline (C_5-C_{12}) and diesel (C_9-C_{22}) based on the product alkane carbon number (Fig. 1C,D). Interestingly, hydrocracking is the most selective route to gasoline in the 250 – 375 °C temperature range. Hydrogenolysis shows a nearly linear increase of gasoline yield with increasing reaction temperature while being less selective overall. In contrast, hydrogenolysis is superior to hydrocracking for diesel production. Only one recent report[16] shows an appreciable yield, comparable to hydrogenolysis, of light diesel-range alkanes over a $Pt/WO_3/ZrO_2$ catalyst under mild reaction conditions without a strong-solid acid. Overall, hydrocracking leverages the acid functionality to crack faster and produce lighter products. Lubricants and waxes are less commonly reported as main products[9,15,16].

It is hard to compare the yields of different products since they change during the reaction and limited such time-dependent data has been published as batch experiments are time consuming. Selectivity-conversion curves are often used to compare catalysts, and this would be a good metric for future reports. Figure 2 shows conversion-selectivity data for various catalysts tested for LDPE hydroconversion at 250 °C with the same LDPE substrate (M_w ~76 kDa) by varying the reaction time from 0.5 to 16 h. Light C_1-C_4 gas, gasoline, and diesel carbon numbers overlap so that the sum can be higher than 100% or lower due to heavy waxes/lubricants with carbon numbers larger than gasoline and diesel. Hydrocracking over $Pt/WO_3/ZrO_2$+HY (Fig. 2A) produces more gasoline than diesel. As the conversion increases, the gasoline selectivity grows from 60 to ca. 75% due to secondary hydrocracking of intermediate C_8-C_{17} hydrocarbons over zeolite acid sites. Without a zeolite (i.e., over $Pt/WO_3/ZrO_2$; Fig. 2B), the gasoline selectivity is nearly independent of the conversion and decreases slightly from 74 to 64.% This catalyst is more selective towards C_8-C_{12} alkanes primarily due to the absence of confinement in the micropores and the milder acidity of the mixed-metal oxide support. The constant product selectivity over a wide range of conversions indicates that chemistry happens primarily on the macromolecule rather than the liquid products. The macromolecules selectively adhere to the catalyst surface and products are generated from the direct cleavage of the chain. This adhesive mechanism segregates the products into the melt bulk, preventing sequential cracking reactions. The difference between Pt to Ru on otherwise identical WO_3/ZrO_2 support (Fig. 2B,C) underscores the importance of the metal on product selectivity. Ru forms heavier products than Pt. For the $Ru/WO_3/ZrO_2$ catalysts (Fig. 2B,C), light gases are seen early on, but the selectivity to liquids improves significantly with increasing conversion. This behavior is due to the gradual deconstruction of LDPE to heavy products that remain in the solid state upon quenching, while methane is cleaved directly from the polymer chain. The selectivity to gasoline and diesel ranged products increases only when the solid product's molecular weight distribution begins to fall into this hydrocarbon range. Since conversion is calculated based on the total solid yield, it misses transformations within the solid, leading to high apparent selectivity to methane. We propose to compare the selectivity to light gases at longer times when conversion is sufficiently high to minimize this issue.

Energy Analysis

Energy use is a valuable metric of chemical processes. These estimations have become even more important due to a shift from traditional performance metrics to sustainability metrics, CO_2 emissions, and climate impact[29]. Moreover, such comparisons can provide valuable insights into the limitations of the technologies and guide the next generation of engineered processes. Despite these benefits, energy analyses for the hydroconversion of polyolefins are lacking. Meanwhile, in recent years, there has been an explicit preference for low-temperature catalytic processes as more environmentally friendly.

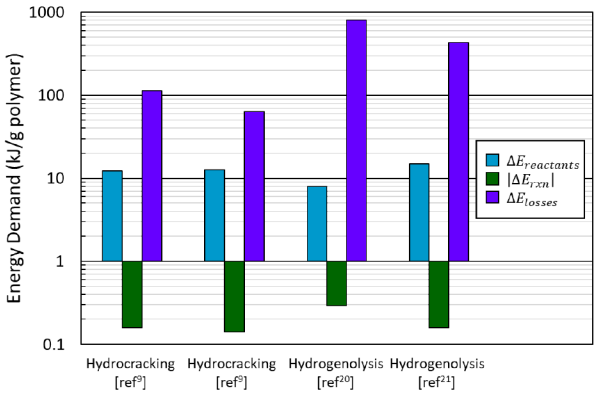

Figure 3. Relative contributions of energy terms for hydrocracking and hydrogenolysis in laboratory reactors. Blue: energy to bring reactants to reaction conditions; green: *absolute value* of reaction energy; and purple: energy lost to the surroundings for laboratory reactors (see text).

We conducted energy balance calculations using data extracted from literature[9,13–15,19–22,24,25] for the hydrocracking and hydrogenolysis of PE and PP. These calculations utilize Eq-1. Here, $\Delta E_{reactants}$ represents the energy needed to bring the reactants (i.e., PE or PP and H_2) from the standard state (25 °C, 1 bar) to reaction conditions, ΔE_{rxn} represents the energy of reaction to produce a product distribution at reaction conditions, and ΔE_{losses} is an estimate of the energy lost to the surrounds over the total reaction time, assuming all reactions were ran in a cylindrical, non-insulated 50 mL batch reactor with a radius of 9 cm and a height of 10 cm. The SI provides details on the calculation of the energy.

$$\Delta E_{demand} = \Delta E_{reactants} + \Delta E_{rxn} + \Delta E_{losses} \quad (1)$$

These calculations could include the energy demand for downstream processes (i.e., separations) to produce commercial products. However, we refrain from doing this to maintain a fairer comparison as the dominant product fractions differ between hydrocracking and hydrogenolysis (Fig. 2). Downstream analysis should be reserved for comparing processes within the same hydroconversion technology.

The typical breakdown in Eq-1 is shown in Fig. 3. Most of the energy in the PO hydroconversion is spent bringing the reactants (polymer and hydrogen) to reaction conditions and heat losses to the surroundings. These contributions dominate the energy of the reaction in Eq-1 by two orders of magnitude. This is because hydroconversion reactions are slightly exothermic (~-50 kJ/mol product) and subsequently do not contribute significantly to the energy makeup. As reactors are scaled up, the heat loss declines. The primary energy consumption is to heat the plastic and hydrogen to reaction conditions (i.e., heating the polymer and hydrogen, melting the polymer, heating the melt, and compressing the hydrogen). The energy of fusion of the plastic is ca. 3% of the energy of heating and compressing the reactants; thus, the phase change energy can be left out for rough estimates. Furthermore, the identity of the plastic (PP vs. PE) negligibly affects the value of $\Delta E_{reactants}$ but significantly alters the hydroconversion products, particularly for hydrogenolysis[20,22,23].

Figure 4A shows the calculated power demand normalized by polymer mass for PO hydrocracking and hydrogenolysis as a function of reaction temperature. There is an apparent increase in the power with increasing reaction temperature for both hydrocracking and hydrogenolysis. Moreover, the power for all hydroconversion processes vs. temperature exhibits a generalizable trend, regardless of variations in the H_2 pressure and/or reaction times. This is consistent with the aforementioned trend toward lower temperature processes[30], and again, more active catalysts are desired to reduce the temperature and the processing time.

The total energy demand vs. temperature (Figure 4B) does not show a clear correlation between variables. There is a large (an order of magnitude) variation in energy demand among studies. Furthermore, it becomes evident that lower reaction temperatures are not necessarily less energy-intensive than higher temperatures because mild processes require longer times to convert the polymer completely (Fig. 4B). Fig. 4B shows clustering of the hydrocracking and hydrogenolysis data, with hydrocracking requiring less energy to deconstruct both PP and PE compared to hydrogenolysis. Reactions that require longer times suffer higher losses to the surroundings, thereby increasing the energy demand. Interestingly, hydrocracking at mildly high temperatures (~330 °C, ref[15]) has the lowest energy demand due to the shorter reaction times because reaction rates grow rapidly with temperature. This finding highlights that high-temperature processes can be beneficial for low-energy PO deconstruction as long as the selectivity can be controlled.

The energy demand as a function of liquid (C_6 – C_{40}) productivity (Fig. 4C) clarifies the segregation between hydrocracking and hydrogenolysis seen in Fig. 4B. In Fig. 4C, all

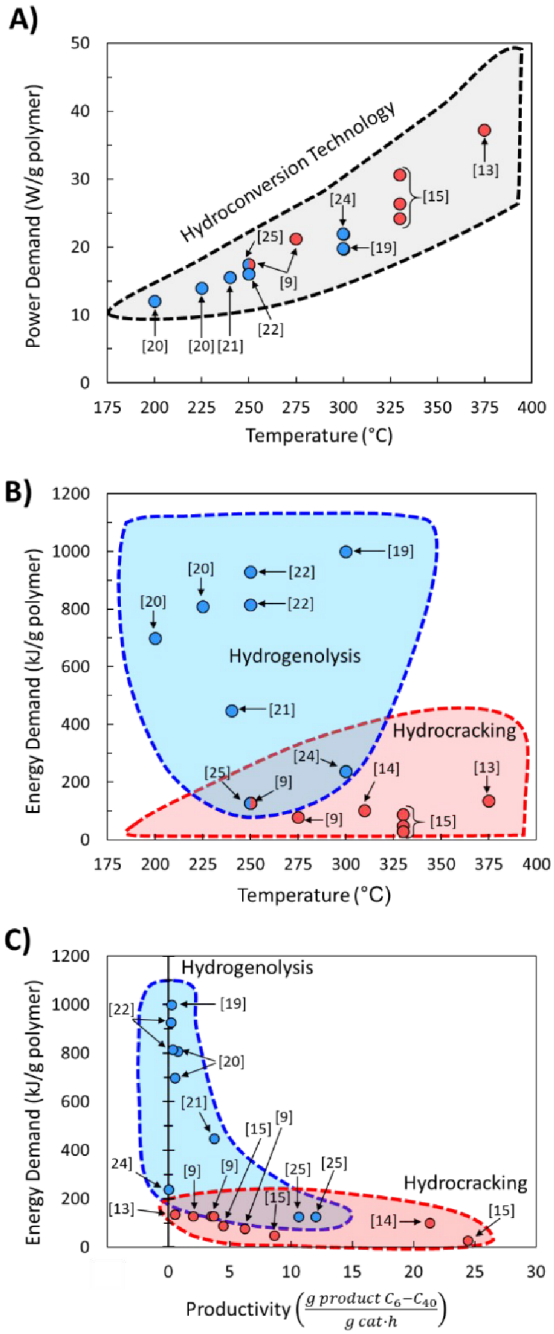

Figure 4. Correlations for laboratory reactors for A) power demand and reaction temperature; B) energy demand and temperature; and C) liquid productivity and energy demand for recent polyolefin hydroconversion literature.

hydroconversion processes fall onto a monotonically decaying curve, but there is again clustering, with hydrocracking having, in general, better productivities (i.e., higher deconstruction rates) compared to hydrogenolysis. The differences in productivity are associated with differences in chemistry and its impact on the relative rates of deconstruction. In hydrogenolysis, mild C-C bond cracking occurs via metal-bound

carbonaceous species, while C-C bond cleavage is mediated by fast carbocation chemistry in hydrocracking. The differences in the mediated reactive species make hydrocracking faster, therefore reducing the overall time needed for polyolefin deconstruction and the subsequent energy demand and improve productivity by limiting the generation of undesirable light gases (i.e., methane). The attainable range of carbon numbers differs between processes, as hydrocracking is restricted to branched C_4–$C_{\sim16}$ products[9,15,16] while hydrogenolysis produces heavier normal alkanes (C_{10+})[20,21,25].

This analysis alludes to future directions for hydrogenolysis and hydrocracking. For hydrocracking, one should engineer catalysts operating at mild temperatures while maintaining high rates and expanding the range of hydrocarbon products. As for hydrogenolysis, future work should enhance the deconstruction rates under the prevalent reaction temperatures and pressures while limiting light gas ($C_1 - C_5$) production. For instance, our recent report[25] shows that hydrogenolysis over a $Ru/WO_3/ZrO_2$ catalyst can breach the current productivity limit to enter the hydrocracking area in Fig. 4C.

Mechanistic Knowledge Transfer and Plastic Surrogates

It is well known that the surface of heterogeneous catalysts responds to and is significantly altered by the reaction environment[31]. Only in rare instances[32] information on active sites and intermediates can be transferred from low- to high-pressures. The connection of ultra-high vacuum and reactor conditions has been a long-standing hope of the scientific community. Still, decades of research have demonstrated that this happens only on certain occasions. A similar mechanistic gap exists in linking model small alkane conversion over metal or metal/acid catalysts to melted polymers under high hydrogen pressure. We elaborate on this point next.

1. Hydrogenolysis

1.1. The nature of catalyst-reactant interactions

Hydrogenolysis catalysts should facilitate the breaking of C-C bonds in alkanes/polyolefins and the H-H bond in H_2 with the subsequent formation of two new terminal C-H bonds in the products. The degree of compensation (χ) allows to estimate the efficiency of this bond redistribution[33]:

$$\chi = \frac{\sum_i D_i - E_a}{\sum_i D_i} \cdot 100\%,$$

where $\sum_i D_i$ is a sum of all broken bond energies and E_a is the activation energy for hydrogenolysis. For most catalysts, χ equals 85-90%[34]. Using standard bond energies[35], we can estimate the hydrogenolysis activation energy over good catalysts to be 80-120 kJ/mol. This estimation quite accurately predicts the minimum E_a[36], while for poor catalysts, it can be much larger than 120 kJ/mol.

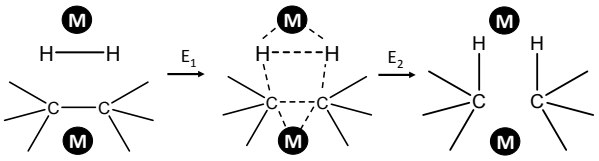

Scheme 2. Formation of adsorbed complex during alkane hydrogenolysis though interaction with two metal sites.

Several attempts were made to estimate the optimal catalyst-alkane interaction energy and maximize the reaction rate.[33] Following ref[33], we can consider the formation of the surface complex according to Scheme 2. This hypothetical scheme reflects that forming carbon-metal bonds weakens the C-C bond in an alkane[37]. If the surface complex contains two metal atoms, then we can estimate the activation energy required in the first step in Scheme 2 using bond energies:

$$E_1 = 2D_{M-H} + 2D_{M-C} - D_{C-C} - D_{H-H}.$$

Here D_{M-H} and D_{M-C} correspond to metal-hydrogen and metal-carbon residue bonds. In the second step, one has the decomposition of the adsorbed complex into products:

$$E_2 = 2D_{C-H} - 2D_{M-C} - 2D_{M-C}.$$

When $E_1 = E_2$, we can easily estimate the total bond energies for metal-hydrogen and metal-carbon residue bonds as:

$$D_{M-H} + D_{M-C} = \frac{2D_{C-H} + D_{C-C} + D_{H-H}}{4} \cong 408\ kJ/mol \quad (2).$$

In the case of low metal-hydrogen bond energy, Eq-2 leads to D_{M-C} of ~408 kJ/mol. Considering the spontaneous dissociation of hydrogen over several metal catalyst sites:

$$D_{M-C} = \frac{2D_{C-H} + D_{C-C}}{4} \cong 290\ kJ/mol \qquad (3).$$

This simple approach reflects the Sabatier principle where too strong carbon-metal binding leads to a very stable adsorbed complex and impede hydrogenolysis rates. Knowledge of the structure of this complex can allow one to compute the exact optimal metal-carbon binding energy. Eq-2 and 3 should be modified if the detailed structure of adsorbed complex and types of bonds being broken and formed are known[38]. A similar concept was used by Sinfelt[39] and Zimmer et al.[40] to explain ethane and larger alkanes reactivity over different metals. For Au, low rates correlate with a lower D_{M-C} leading to a slow first step in Scheme 1. For Pt, Ir, and Os, D_{M-C} values fall in the optimal range. In moving from Os to Re, strong metal-carbon binding reduces the rate of the second step in Scheme 2. With this concept, several model metal surfaces can be screened computationally to identify metal-carbon binding energies that follow Eq-2 or 3.

For Pt-catalyzed hydrogenolysis of neopentane[41], the authors show using DFT that Pt 5d electrons are primarily responsible for Pt binding to the alkyl radical, while the Pt 6sp electrons are involved in the Pt-H bond. Different supports for Pt clusters can significantly alter the electron densities on those orbitals. Thus, metal-support interactions can effectively change D_{Pt-H} and D_{Pt-C} on the left side of Eq-2 or Eq-3. This change in bond energies induced by metal-support interactions can reduce the Pt activity.

Sinfelt compared the hydrogenolysis activity of different metals as a function of their d-band filling[42]. He observed an activity maximum at a certain level, roughly estimated from the position of the metal in the periodic table. We can speculate that D_{M-C} is influenced by the relative number of d-electrons, similar to Pt. So, the dependence on the d-character of the metal may also reflect the optimal D_{M-C} values.

Another interesting consequence of Eq-3 is a different optimal D_{M-C} for the hydrogenolysis of various bonds in the PO

chain. For example, using the data from ref[43], we can estimate that D_{M-C} should be different for C^2-C^2 internal bond breaking in PE or for C^3-C^1 bonds in PP. Obviously, multiple adsorbed complexes can exist on the surface at the same time leading to a much more complicated reaction network. Yet, these simple principles are powerful for a basic analysis and design.

1.2. Small alkane hydrogenolysis kinetics

Detailed studies on alkanes hydrogenolysis for various substrates were reported by Flaherty et al.[44–46]. Here we aim only to highlight select concepts and lessons accumulated in the vast hydrogenolysis literature over the years. Hydrogenolysis involves C-H bond breaking by dissociative adsorption:

$$C_nH_{2n+2} + zS \leftrightarrow C_nH_x + (2n+2-x)H_{ads}.$$

This is considered quasi-equilibrated and consists of several dehydrogenation elementary steps. The C_nH_x formation is followed by C-C bond breaking:

$$C_nH_x \rightarrow C_aH_b + C_{n-a}H_{x-b}.$$

Bond breaking is frequently recognized as the rate-determining step leading to the following TOF[41]:

$$TOF = k\theta_C\theta_H^{\alpha} \qquad (4),$$

where θ_C and θ_H are surface coverages of C_nH_x and adsorbed H_{ads}, respectively. The reaction order α characterizes the number of H_{ads} before C-C bond breaking.

The C-H bond breaking equilibration is based on the fast H/D exchange rates between alkanes and D_2 under hydrogenolysis conditions and multiple observations of highly stable dehydrogenated species[39]. Surface science studies show that small alkanes dissociation to C_nH_x and H_2 on metal surfaces is orders of magnitude faster than hydrogenolysis. After connecting the dehydrogenation equilibrium with the rate in Eq-4, the TOF dependence on θ_H is[41]:

$$TOF = k_1\theta_H^{\alpha}(1-\theta_H)^z p_C p_H^{\frac{x}{2}-n-1}.$$

Here $(1-\theta_H)^z$ corresponds to the probability of z surface sites being free of H_{ads} to accommodate the C_nH_x intermediate, and p_C and p_H are the partial pressures of the alkane and hydrogen, respectively. One can correlate θ_H to p_H using the Langmuir isotherm[43]:

$$1-\theta_H = \frac{1}{\sqrt{K_H p_H}},$$

leading to Eq-5:

$$TOF = k_2 p_c p_H^{\frac{x-z}{2}-n-1} \qquad (5).$$

This model indicates a first-order dependence on the alkane pressure and a negative reaction order on hydrogen. Constant negative orders for hydrogen at p_H>20 bar and 320 °C for n-C_8 – C_{10} alkanes over an Ir catalyst have been reported[47]. The apparent hydrogen order is close to -3. This is explained by Eq-5 due to the reduced probability of finding z active sites to bind C_nH_x at high hydrogen coverages. This model explains the hydrogenolysis activity over Pt and Ni in certain cases[41,48]. When the number of surface sites involved in C_nH_x binding is known, one can estimate the degree of dehydrogenation, i.e., the number of H atoms removed from the initial alkane, prior to C-C bond breaking. Analysing the ethane TOF dependence on p_H, using an equation similar to Eq-5, Boudart[43] estimated that 4 Ni and 2 Fe surface sites are required for hydrogenolysis, respectively.

Several authors[41,48] reported that the Langmuirian isotherm is inadequate to describe the θ_H vs. p_H dependence, and the Temkin isotherm: $\theta_H \sim \alpha log(p_H)$ is more suitable for non-ideal surfaces. This approach leads to an interesting nonlinear dependence of the apparent reaction orders and activation energy on hydrogen coverage with a sharp maximum[49].

An essential limitation of Eq-5 is that the surface coverage of C_nH_x is calculated assuming dehydrogenation equilibrium. Leclercq et al.[50] derived Eq-6 in better agreement with experimental data at moderate hydrogen pressures:

$$TOF = \frac{k_3 p_C p_H}{k_C p_C + k_H^{\frac{z}{2}} p_H^{n+1+\frac{z-x}{2}}} \qquad (6),$$

where k_C and k_H are the adsorption coefficients for the alkane and hydrogen, respectively, z is the number of surface sites involved in the binding of the alkane. Several similar equations were proposed in the literature[51]. At high p_H or high H_{ads} coverage, the second term in the denominator of Eq-6 dominates, leading to the simplified Eq-7, which is very similar to Eq-5:

$$at\ high\ H_{ads}: TOF = k_4 p_C p_H^{\frac{x-z}{2}-n} \qquad (7).$$

At low hydrogen pressures or low H_{ads} coverage, Eq-6 yields:

$$at\ low H_{ads}: r = k_5 p_H \qquad (8).$$

In this case, a zero-order dependence on hydrocarbon and a first-order dependence on hydrogen are expected[52]. Differentiation of Eq-6 gives the hydrogen pressure for a maximum reaction rate:

$$p_H^{max} = k_6\left(\frac{p_C}{2n-x+z}\right)^{\frac{2}{2n+2+z-x}} \qquad (9).$$

Eq-9 and 6 show that the optimal hydrogen pressure required to achieve TOF_{max} increases with p_C. Indeed, hydrogenolysis rates typically have a maximum with varying hydrogen pressure[53]. Bond et al. highlighted that for catalysts with very strong hydrogen chemisorption, the maximum TOF could shift to lower pressures.

The pool of dehydrogenated surface compounds can isomerize to each other. Additionally, all surface species can participate in C-C bond breaking with different selectivity and rates. Furthermore, these key intermediates change with the metal catalyst. For instance, Hibbitts et al.[37] showed that [CH_2-CH_3] has the lowest C-C bond breaking activation energy in ethane hydrogenolysis over Cu, whereas on Ir and Ru [CH-CH_2] is the most reactive intermediate. Dumesic[54,55] and Vlachos[56] showed that microkinetic modeling parametrized with DFT calculations could capture the most reactive C_nH_x species. Microkinetic modeling also considers the hydrogen and alkyl coverage effects, which are hard to account for using simpler approaches[41] that lead to various approximate rate expressions.

While microkinetic models are feasible for small hydrocarbons, they are a formidable task for polymers.

Finally, the hydrogenolysis rate often has a negative order dependence on the hydrogen pressure, but for some hydrocarbons, a maximum is seen. Simplistically, the reaction order is related to the structure of the C_nH_x intermediate corrected to the number of surface sites. Deviation from the Langmuirian isotherm usually leads to a substantial variation of the apparent activation energy with temperature due to coverage effects.

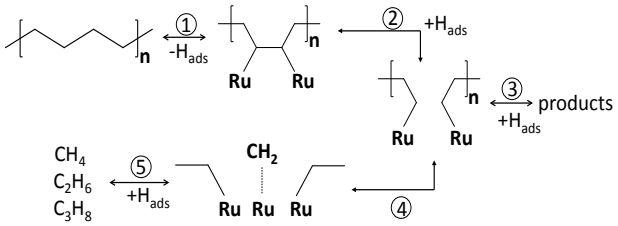

Scheme 3. Reaction network of PE hydrogenolysis over $Ru/WO_3/ZrO_2$ catalyst [24]. 1) dehydrogenation; 2) C-C bond breaking; 3) hydrogenation with products desorption; 4) secondary hydrogenolysis; 5) formation of light gas products.

1.3. Mechanistic comparison of PO and small alkane hydrogenolysis

There are intriguing similarities of PO hydrogenolysis to and differences from small alkanes. Ru and Pt-based catalysts were studied for PE[20,21,25] and PP[22,23] hydrogenolysis in the melt phase at 200-300 °C at H_2 pressure above 10 bar. Ru particles on carbon, TiO_2, and CeO_2 show superior activity to other metals, resembling the catalyst activity trend of ethane hydrogenolysis[42].

In small alkane hydrogenolysis, the hydrogen reaction order is essential, and so is for macromolecules. For lighter normal C_2-C_{10} alkanes, the hydrogen reaction order is usually negative (approx. -3[44–46]). As discussed above, this implies an equilibrated alkane dehydrogenation and competitive substitution of C_nH_x with H_{ads} over surface sites at high p_H.

In PE conversion over $Ru/WO_3/ZrO_2$ catalysts, the liquid yields grow when p_H increases from 25 to 130 bar[25]. A similar effect occurs on Ru/C upon a pressure increase from 15 to 25 bar[20]. This indicates that the hydrogen order in PE hydrogenolysis is positive, corresponding to Eq-6 or 8. The stronger binding of the polymer leads to depletion of H_{ads} species, making the response different from the lighter alkanes. A high hydrogen pressure should rather promote the C-C breaking in accordance with Eq-4. This effect is not specific to polymers, and was previously observed for cycloalkanes at p_H below 20 bar [46]. The strong binding of polymers to metal surfaces changes the extent of secondary reactions. The methane production can strongly be modulated with p_H, due to the strong binding of the polymer with C_nH_x intermediates undergoing secondary hydrogenolysis to methane. This sequence is depicted as steps 4 and 5 in **Error! Reference source not found.** Similar observations were previously made for n-C_6 and i-C_6 hydrogenolysis over Ru/Al_2O_3[57]. High hydrogen coverages hydrogenate the C_nH_x reaction intermediates followed by desorption of the hydrocarbons, reducing their time on the surface after the primary C-C bond breaking (step 3 in Scheme). At low hydrogen coverages, C_nH_x residues stay longer and crack further, leading to light alkanes (steps 4 and 5). This pressure dependence and learnings from small hydrocarbons provide a knob for methane suppression in PO hydrogenolysis. Specifically, catalysts with a stronger H bonding or an H reservoir and higher pressures improve the selectivity to liquids. For instance, polytungstate domains on the $Ru/WO_3/ZrO_2$ surface serve as reservoirs for hydrogen due to the partial WO_x reduction. These reduced WO_x species lead to higher liquid yields similar to using higher hydrogen pressures[26].

Van der Waals interactions will increase with each additional CH_2 group leading to stronger polymer binding compared to small alkanes. On the other hand, chemisorption on the catalyst surface, multisite binding and other factors can significantly impact the energetics of adsorbed intermediates.

An important deviation from the classic hydrogenolysis is the hypothesis of quasi-equilibrated dehydrogenation steps. It may be true for polymers in certain instances. Recent results[23] show that PP hydrogenolysis over Ru/TiO_2 in D_2 leads to the formation of evenly deuterated liquid products. At the same time, the solid residues only have significant deuteration in [CH_2] groups, but not in [CH_3]. This indirectly indicates that the rates of [CH_3] group dehydrogenation are almost comparable to the rates of C-C bond hydrogenolysis. One possible explanation invokes the multisite binding of PP during surface

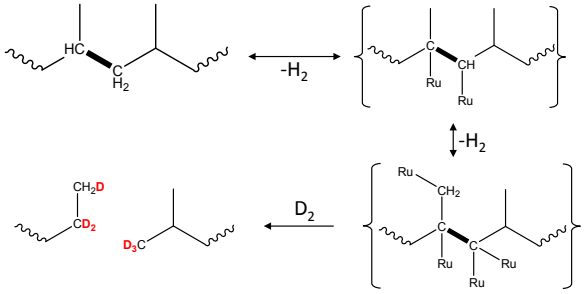

Scheme 4. Surface intermediates during PP hydrogenolysis explain similar rates of C-C bond breaking and H/D exchange in CH_3 group over Ru/TiO_2 catalyst. Reprinted with permission from ACS Catal. 2021, 11, 13, 8104–8115. Copyright 2021 American Chemical Society.

dehydrogenation (Scheme). To sufficiently reduce the strength of C-C bonds, multiple Ru-C contacts should form not only in nearest C atoms, but also at the CH_3 group. Formation of this intermediate can be challenging. After slow dehydrogenation, the internal C-C bond breaking can have a similar or even higher intrinsic rate.

To recap, we postulate that PO hydrogenolysis has several distinct features:

- PO chemisorption is stronger than hydrogen leading to a positive apparent reaction order with respect to p_H
- Due to stronger macromolecule binding, secondary

reactions are more influential for selectivity, compared to small alkanes
- Dehydrogenation and C-C bond breaking rates can be comparable. The formation of multiple constrained Ru-C bonds is necessary for C-C bond breaking.

2. Hydrocracking

2.1 Hydrocracking of model alkanes

The literature on hydrocracking of model alkanes is vast; here, we describe some key aspects related to PO hydrocracking (Fig. 5)[58–63]. Hydrocracking requires bifunctional catalysts with metallic and acidic sites. Metallic sites dehydrogenate paraffin species to olefins. These olefins then diffuse to Brønsted acid sites that catalyze skeletal isomerization and β-scission (i.e., C-C cracking) reactions via well-established carbenium ion chemistry[59–61,64]. Finally, the metallic sites hydrogenate the olefins produced from the acid-catalyzed reactions to final alkanes. The entire cycle keeps repeating itself.

Key reaction parameters[60,65–68] in model alkanes (i.e., temperature, H_2 pressure, alkane chain length, etc.) and catalyst descriptors[62,69–75] (i.e., metal-acid balance, intimacy between sites, site accessibility, etc.) have been identified. The concept of ideal and nonideal hydrocracking is typically utilized to describe the effects of these variables[60,63]. The ideal hydrocracking is characterized by 1) symmetric product distribution centered around half of the feedstock carbon number; 2) high selectivities to isomerized products; 3) acid-catalyzed reactions being rate-limiting; and 4) a reaction mechanism that converts the alkane feedstock sequentially to monobranched isomers, then dibranched isomers, and finally cracked products. Conversely, nonideal hydrocracking is characterized by 1) a highly left-skewed product distribution typically with large fractions of C_3 and C4 alkanes; 2) low selectivity to isomerized products; 3) metal-catalyzed reactions being rate-limiting; and 4) a reaction mechanism that produces isomerized feedstock species and cracked species simultaneously.

Interestingly, the effect of system variables on the hydrocracking performance is captured well with the ideal/non-ideal hydrocracking regimes. For example, Thybaut et al.[65] showed that high reaction temperatures, low reaction pressures, and high molar hydrogen-to-hydrocarbon ratios pushed n-dodecane hydrocracking to the nonideal regime. Their detailed kinetic analysis showed these parameters alter the reaction network in different ways. Specifically, higher reaction temperatures primarily increase the relative rates of acid-catalyzed and metal-catalyzed reactions. In contrast, low total pressures have a thermodynamic effect, impacting the concentration of the reactive intermediates (alkenes and therefore carbocations). Despite mechanistic differences, altering these parameters ultimately enhances the β-scission rates to lighter alkanes with less branching.

2.2 Applying Concepts from Alkane Hydrocracking to PO

The model alkane literature provides an excellent foundation for designing PO hydrocracking catalysts. However, it is unclear if the relationships in model alkanes are valid for PO feedstocks. Our recent work[16], investigating the metal-acid balance (i.e., the metal-to-acid site molar ratio) and its role in LDPE hydrocracking, highlights many parallels between the model alkane and PO, such as the shift from type-B to type-A β-scission as the metal-acid balance increases. Additionally, we discovered crucial phenomena in LDPE hydrocracking absent from model alkane systems, such as the adhesive-like polymer adsorption to the catalytic surface, which significantly alters the hydrocracking dynamics.

Subsequently, we need to understand the nature of polymer adsorption in reactive environments through comparative studies to probe key reaction parameters, identify catalyst descriptors, and bridge the gap between model alkanes and POs. Polymer diffusion is an essential topic in PO hydrocracking as several authors[58,72–75] have highlighted the importance of mass transfer between the catalytic sites in the hydrocracking of alkanes. For example, Oenema et al.[72] demonstrated the intimacy (i.e., distance) between solid acid and Pt sites supported on different zeolites directly impacts the cracking and isomerization selectivities of n-C_7 hydroisomerization. The authors reported optimal isomerization selectivities with site

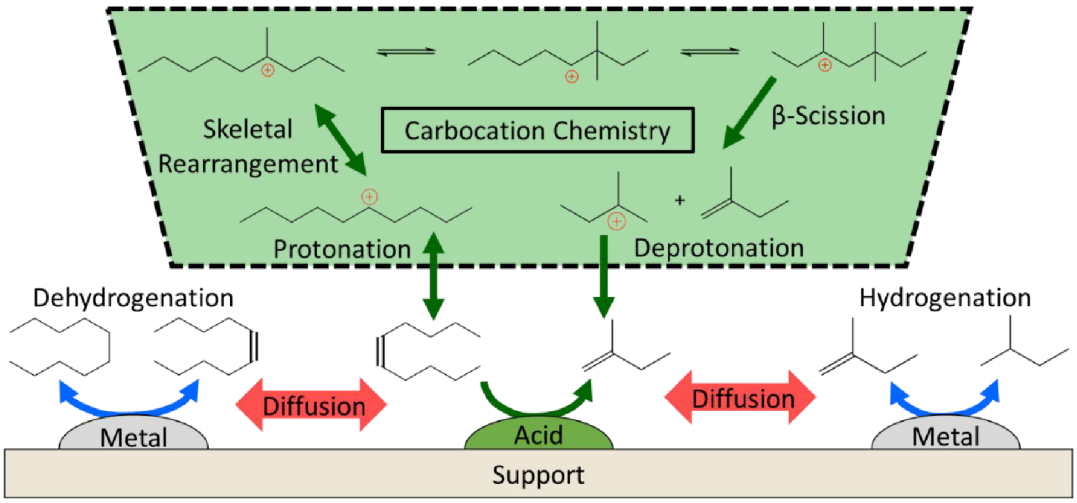

Figure 5. Overview of the reaction mechanism for the hydrocracking of small alkanes over a metal-acid bifunctional catalyst.

intimacies in the nanoscale range for large pore zeolites; closest intimacies suffer from cracking reactions, whereas microscale separation reduces the activity and isomer selectivity due to the heptene concentration gradients. We believe mass transfer effects are likely compounded in the PO hydrocracking due to the complex polymer physics and are further influenced by the polymer structure. For example, in LDPE hydrocracking over Pt/USY, severe overcracking to C_3 – C_6 alkanes has been observed[9,15]. This catalytic behavior is likely due to the confinement of polymer chains in the zeolite pores, which restrict chain removal and result in excessive cracking. Thus, confinement effects and the diffusion r of polymers are an important area for further studies to further bridge the gap between PO and model alkanes.

It is crucial to note that the concept of (non)ideality has limited applicability in characterizing PO hydrocracking because of the distinct differences in the product distributions and the reaction mechanisms compared to alkane hydrocracking. Analysis of the symmetry/skewness is employed to determine (non)ideality[63]. In PO hydrocracking, the product distributions across all products (gases, liquids, and solids) are asymmetric, i.e., PO hydrocracking processes are highly nonideal. Our work on LDPE hydrocracking[16] demonstrates this feature as the entire carbon number distribution continues to be highly left-shifted over the range of metal-acid balances because the extractable (C_1 – C_{35}) products are produced directly from β-scission of the polymer chain. In contrast, changes to the polymer residues are gradual due to their inherent size.

Small alkane hydrocracking follows sequential or concerted networks for ideal and non-ideal systems, respectively, to isomerized and cracked products[61,69,71]. However, isomerization and cracking reactions appear decoupled in PO hydrocracking due to the adhesive adsorption of the polymer to the catalytic surface and the ability to incorporate significant branching in polymer chains that hinders β-scission in the interior[16]. Subsequently, the characteristics of (non)ideal hydrocracking in small alkanes are ill-defined for POs. The terminology should be forgone or revised as more knowledge accumulates.

The Plastics Materials Gap

A challenge in comparing the performance of catalysts owes to the wild variation of the properties and suppliers of virgin polymer materials employed in laboratory studies. The average molecular weight, the density, the degree of crystallinity, and possible impurities even in simple PE, significantly affect the rate of deconstruction and product distribution, rendering comparisons across studies nearly impossible. Fundamental experimental studies and models that can account for these material effects on reaction performance will be essential to close the feedstock materials gap and understand how catalysts interact with and deconstruct polymers. Meanwhile, we propose to use the same virgin materials among laboratories from the same vendors to standardize studies and facilitate benchmarking. For model polyolefins, we suggest Sigma-Aldrich HDPE (427985) for polyethylene substrates and Sigma-Aldrich isotactic-PP (427888) for polyethylene. It is also crucial to thoroughly characterize any polymer feedstock used for reactions. ^{13}C NMR can be used to deduce branching density, GPC or MALDI to estimate molecular weight distributions, and GC-MS analysis to assess the type and concentration of additives and stabilizers.

Furthermore, we propose studies to regularly characterize the polymer residues using gel-permeation chromatography (GPC), differential scanning calorimetry (DSC), and ^{1}H and ^{13}C nuclear magnetic resonance (NMR) to report changes in the neat polymer.

The complex nature of plastic waste, especially of packaging materials, has been extensively highlighted recently[6,76]. Packaging materials contribute to ca. 40% of all waste and contain a substantial amount of PE or PP, but also other functionalized polymers and inorganic additives constitute several percent of the total material.

The effect of additives on catalyst performance has never been studied systematically in the open literature. Nonetheless, existing literature indicates the severity of additives[77]. For example, a small fraction (14%) of EVA (ethylene vinyl acetate) leads to a significant decrease of Al-MCM-41 activity in the LDPE cracking at 420 °C[77]. Interestingly, the inhibiting effect was not connected with the release of acetic acid. High-temperature decarboxylation of EVA produces polyene chains, which readily polymerize and cross-link into extended coke species. It was proposed that the microporous environment of ZSM-5 prevents extensive coking, leading to stable cracking performance. These phenomena can significantly change the entire research strategy for optimal catalysts and need to be considered.

Conclusions

Low-temperature hydroconversion processes have come to the forefront of catalytic research for the deconstruction of polyolefin (PO) plastic waste to fuels, lubricants, and waxes. Despite the progress, several unconventional challenges prevent direct comparison of results between laboratories and the rapid acceleration of catalyst and process development. Some of them include the varying and complex feedstock (composition, density, structure, etc.), impurities and additives, the different nature of polymer adsorption on the catalyst surfaces, the larger diffusion limitations, the presence of a melt phase or a solvent, analytical challenges, etc.

In this comparative review, we highlighted fundamental insights into the hydrogenolysis and hydrocracking of model alkanes as a framework to engineer better catalysts and processes. We compared the results from small alkanes and PO feedstocks to identify major hurdles that currently hinder catalyst design. For hydrogenolysis, the key takeaways are:

- Polyolefins binding over metal active sites is stronger than small alkanes. This leads on one hand to a positive reaction order for hydrogen, and on the other, to strongly bonded intermediates that participate in secondary fragmentation leading to excessive quantities of light hydrocarbons.
- The classical concept of equilibrated dehydrogenation steps preceding the C-C bond breaking seems invalid for some polymers compared to small alkanes.

- Computational screening of metal—polymer surface complexes in search of optimal interaction strength can help to further catalyst development.
- Tuning of the metal electronic structure and its d-band closer to the optimum may allow selective targeting of different C-C bonds (C^1-C^2 vs. C^2-C^2 vs. C^2-C^3, etc.) in polyolefins.

For hydrocracking processes, key takeaways are:

- The impact of key reaction parameters and bifunctional catalyst descriptors need to be understood.
- The key differences of small alkanes and PO hydrocracking need to be delineated.
- The role of mass transfer and its effects on hydrocracking performance needs to be revealed.

Additionally, we analysed the energy consumption of the existing PO hydrocracking and hydrogenolysis technologies to draw a fairer comparison between these processes and provide broad guidance. Based on this analysis, future hydroconversion should:

- Engineer hydrocracking catalysts capable of maintaining high deconstruction rates at mild temperatures.
- Expand the feasible product distribution of PO hydrocracking to larger hydrocarbons.
- Enhance the hydrogenolysis deconstruction rates under the prevalent reaction temperatures and pressures while limiting light gas formation.

Finally, we have proposed fundamental studies, benchmarking, and standardization guidelines such as:

- Investigate the role of the polymer attributes (i.e., average molecular weight, density, degree of crystallinity) in PO deconstruction.
- Examine the impact of additives on catalyst performance and develop mitigation strategies.
- Standardize the virgin materials (same vendors, molecular weight, etc.) among laboratories.
- Characterize the polymer residues using GPC, DSC, and NMR techniques.
- Report turnover numbers and location of broken C-C bonds.

We believe these endeavours are necessary for the progress of plastic waste deconstruction technologies and will significantly contribute to addressing the global threat of plastic waste.

Author Contributions

Manuscript has been written by equal contribution of all authors.

Conflicts of interest

There are no conflicts to declare.

Acknowledgements

The University of Delaware Center for Plastics Innovation is supported by the U.S. Department of Energy (DOE), Office of Science, Basic Energy Sciences under Award Number DE-SC0021166. Any opinions, findings, conclusions or recommendations expressed in this material are those of the authors and do not necessarily reflect those of the DOE. B.C.V. acknowledges a Graduate Research Fellowship through the National Science Foundation under Grant Number 1940700.

Notes and references

1 L. Lebreton and A. Andrady, *Palgrave Commun.*, 2019, **5**, 1–11.
2 J. J. Klemeš, Y. Van Fan and P. Jiang, *https://doi.org/10.1080/15567036.2020.1801906*, 2020, **43**, 1549–1565.
3 R. Geyer, J. R. Jambeck and K. L. Law, *Sci. Adv.*, , DOI:10.1126/sciadv.1700782.
4 P. F. Britt, G. W. Coates and K. I. Winey, in *Basic Energy Sciences Roundtable*, 2019, pp. 1–56.
5 A. J. Martín, C. Mondelli, S. D. Jaydev and J. Pé Rez-Ramírez, *CHEMPR*, , DOI:10.1016/j.chempr.2020.12.006.
6 L. D. Ellis, N. A. Rorrer, K. P. Sullivan, M. Otto, J. E. McGeehan, Y. Román-Leshkov, N. Wierckx and G. T. Beckham, *Nat. Catal. 2021 47*, 2021, **4**, 539–556.
7 X. Chen, Y. Wang and L. Zhang, *ChemSusChem*, , DOI:10.1002/CSSC.202100868.
8 J. Garcia-Martinez, *Angew. Chemie Int. Ed.*, 2021, **60**, 4956–4960.
9 S. Liu, P. A. Kots, B. C. Vance, A. Danielson and D. G. Vlachos, *Sci. Adv.*, 2021, **7**, eabf8283.
10 L. D. Ellis, S. V. Orski, G. A. Kenlaw, A. G. Norman, K. L. Beers, Y. Román-Leshkov and G. T. Beckham, *ACS Sustain. Chem. Eng.*, 2021, acssuschemeng.0c07612.
11 C. Y. Chen, • D J O'rear and • P Leung, , DOI:10.1007/s11244-012-9910-3.
12 K. R. Venkatesh, J. Hu, W. Wang, G. D. Holder, J. W. Tierney and I. Wender, *Energy and Fuels*, 1996, **10**, 1163–1170.
13 W. Ding, J. Liang and L. L. Anderson, *Energy and Fuels*, 1997, **11**, 1219–1223.
14 J. M. Escola, J. Aguado, D. P. Serrano, A. García, A. Peral, L. Briones, R. Calvo and E. Fernandez, *Appl. Catal. B Environ.*, 2011, **106**, 405–415.
15 A. Bin Jumah, V. Anbumuthu, A. A. Tedstone and A. A. Garforth, *Ind. Eng. Chem. Res.*, 2019, **58**, 20601–20609.
16 B. C. Vance, P. A. Kots, C. Wang, Z. R. Hinton, C. M. Quinn, T. H. Epps, L. T. J. Korley and D. G. Vlachos, *Appl. Catal. B Environ.*, 2021, **299**, 120483.
17 G. Celik, R. M. Kennedy, R. A. Hackler, M. Ferrandon, A. Tennakoon, S. Patnaik, A. M. Lapointe, S. C. Ammal, A. Heyden, F. A. Perras, M. Pruski, S. L. Scott, K. R. Poeppelmeier, A. D. Sadow and M. Delferro, *ACS Cent. Sci.*, 2019, **5**, 1795–1803.
18 F. Zhang, M. Zeng, R. D. Yappert, J. Sun, Y. H. Lee, A. M. LaPointe, B. Peters, M. M. Abu-Omar and S. L. Scott, *Science (80-.).*, 2020, **370**, 437–441.

19 A. Tennakoon, X. Wu, A. L. Paterson, S. Patnaik, Y. Pei, A. M. LaPointe, S. C. Ammal, R. A. Hackler, A. Heyden, I. I. Slowing, G. W. Coates, M. Delferro, B. Peters, W. Huang, A. D. Sadow and F. A. Perras, *Nat. Catal.*, 2020, 893–901.

20 J. E. Rorrer, G. T. Beckham and Y. Román-Leshkov, *JACS Au*, 2020, jacsau.0c00041.

21 Y. Nakaji, M. Tamura, S. Miyaoka, S. Kumagai, M. Tanji, Y. Nakagawa, T. Yoshioka and K. Tomishige, *Appl. Catal. B Environ.*, 2021, **285**, 119805.

22 J. E. Rorrer, C. Troyano-Valls, G. T. Beckham and Y. Román-Leshkov, *ACS Sustain. Chem. Eng.*, 2021, acssuschemeng.1c03786.

23 P. A. Kots, S. Liu, B. C. Vance, C. Wang, J. D. Sheehan and D. G. Vlachos, *ACS Catal.*, 2021, **11**, 8104–8115.

24 W. T. Lee, F. D. Bobbink, A. P. van Muyden, K. H. Lin, C. Corminboeuf, R. R. Zamani and P. J. Dyson, *Cell Reports Phys. Sci.*, 2021, **2**, 100332.

25 C. Wang, T. Xie, P. A. Kots, B. C. Vance, K. Yu, P. Kumar, J. Fu, S. Liu, G. Tsilomelekis, E. A. Stach, W. Zheng and D. G. Vlachos, *JACS Au*, 2021, **1**, 1422–1434.

26 T. Bligaard, R. M. Bullock, C. T. Campbell, J. G. Chen, B. C. Gates, R. J. Gorte, C. W. Jones, W. D. Jones, J. R. Kitchin and S. L. Scott, *ACS Catal.*, 2016, **6**, 2590–2602.

27 D. Zhao, X. Wang, J. B. Miller and G. W. Huber, *ChemSusChem*, 2020, **13**, 1764–1774.

28 J.-P. Lange, *Nat. Catal. 2021 43*, 2021, **4**, 186–192.

29 J. B. Zimmerman, P. T. Anastas, H. C. Erythropel and W. Leitner, *Science (80-.).*, 2020, **367**, 397–400.

30 P. T. Anastas and J. C. Warner, *Green Chemistry Theory and Practice*, Oxford University Press, Cary, North Carolina, 1998.

31 J. J. Velasco-Vélez, V. Pfeifer, M. Hävecker, R. Wang, A. Centeno, A. Zurutuza, G. Algara-Siller, E. Stotz, K. Skorupska, D. Teschner, P. Kube, P. Braeuninger-Weimer, S. Hofmann, R. Schlögl and A. Knop-Gericke, *Rev. Sci. Instrum.*, 2016, **87**, 053121.

32 R. Imbihl, R. J. Behm and R. Schlögl, *Phys. Chem. Chem. Phys.*, 2007, **9**, 3459–3459.

33 G. I. Levi and A. A. Balandin, *Bull. Acad. Sci. USSR, Div. Chem. Sci.*, 1958, **7**, 1447–1449.

34 G. K. Boreskov, *Heterogeneous catalysis*, Nova Science Publishers, 2003.

35 Y. R. Luo, *Compr. Handb. Chem. Bond Energies*, 2007, 1–1656.

36 G. C. Bond and J. C. Slaa, *J. Mol. Catal. A Chem.*, 1995, **101**, 243–253.

37 A. Almithn and D. Hibbitts, *J. Phys. Chem. C*, 2019, **123**, 5421–5432.

38 F. Zaera and S. Tjandra, *J. Am. Chem. Soc.*, 1996, **118**, 12738–12746.

39 J. H. Sinfelt, *Catal. Letters*, 1991, **9**, 159–171.

40 H. Zimmer, P. Tétényi and Z. Paál, *J. Chem. Soc. Faraday Trans. 1 Phys. Chem. Condens. Phases*, 1982, **78**, 3573–3586.

41 D. C. Koningsberger, M. K. Oudenhuijzen, J. De Graaf, J. A. Van Bokhoven and D. E. Ramaker, *J. Catal.*, 2003, **216**, 178–191.

42 J. H. Sinfelt, *Adv. Catal.*, 1973, **23**, 91–119.

43 M. Boudart, *AIChE J.*, 1972, **18**, 465–478.

44 D. D. Hibbitts, D. W. Flaherty and E. Iglesia, *J. Phys. Chem. C*, 2016, **120**, 8125–8138.

45 D. D. Hibbitts, D. W. Flaherty and E. Iglesia, *ACS Catal.*, 2016, **6**, 469–482.

46 D. W. Flaherty, D. D. Hibbitts and E. Iglesia, *J. Am. Chem. Soc.*, 2014, **136**, 9664–9676.

47 D. W. Flaherty and E. Iglesia, *J. Am. Chem. Soc.*, 2013, **135**, 18586–18599.

48 G. A. Martin, *J. Catal.*, 1979, **60**, 345–355.

49 G. A. Martin, R. Dutartre, S. Yuan, C. Márquez-Alvarez and C. Mirodatos, *J. Catal.*, 1998, **177**, 105–112.

50 G. Leclercq, L. Leclercq and R. Maurel, *Bull. des Sociétés Chim. Belges*, 1979, **88**, 599–620.

51 G. C. Bond, J. Calhoun and A. D. Hooper, *J. Chem. Soc. - Faraday Trans.*, 1996, **92**, 5117–5128.

52 D. W. Flaherty, A. Uzun and E. Iglesia, *J. Phys. Chem. C*, 2015, **119**, 2597–2613.

53 G. C. Bond, *Appl. Catal. A Gen.*, 1997, **149**, 3–25.

54 Simon G. Podkolzin, Rafael Alcala, and Juan J. de Pablo and J. A. Dumesic*, *J. Phys. Chem. B*, 2002, **106**, 9604–9612.

55 R. D. Cortright, R. M. Watwe and J. A. Dumesic, *J. Mol. Catal. A Chem.*, 2000, **163**, 91–103.

56 M. Salciccioli, Y. Chen and D. G. Vlachos, *Ind. Eng. Chem. Res.*, 2010, **50**, 28–40.

57 B. Coq, A. Bittar and F. Figueras, *Appl. Catal.*, 1990, **59**, 103–121.

58 P. B. Weisz, *Adv. Catal.*, 1962, **13**, 137–190.

59 H. L. Coonradt and W. E. Garwood, *Ind. Eng. Chem.*, 1964, **56**, 69–69.

60 J. Weitkamp, *Am. Chem. Soc. Div. Pet. Chem. Prepr.*, 1975, **20**, 489–507.

61 J. A. Martens, P. A. Jacobs and J. Weitkamp, *Appl. Catal.*, 1986, **20**, 239–281.

62 T. L. M. Maesen, S. Calero, M. Schenk and B. Smit, *J. Catal.*, 2004, **221**, 241–251.

63 J. Weitkamp, *ChemCatChem*, 2012, **4**, 292–306.

64 L. A. Wall, S. L. Madorsky, D. W. Brown, S. Straus and R. Simha, *J. Am. Chem. Soc.*, 1954, **76**, 3430–3437.

65 J. W. Thybaut, C. S. Laxmi Narasimhan, J. F. Denayer, G. V Baron, P. A. Jacobs, J. A. Martens and G. B. Marin, *Ind. Eng. Chem. Res.*, 2005, **44**, 5159–5169.

66 H. F. Schulz and J. H. Weitkamp, *Ind. Eng. Chem. Prod. Res. Dev.*, 1972, **11**, 46–53.

67 M. Steijns and G. F. Froment, *Ind. Eng. Chem. Prod. Res. Dev.*, 1981, **20**, 660–668.

68 V. Calemma, S. Peratello and C. Perego, *Appl. Catal. A Gen.*, 2000, **190**, 207–218.

69 G. E. Glannetto, G. R. Perot and M. R. Guisnet, *Ind. Eng. Chem. Prod. Res. Dev*, 1986, **25**, 481–490.

70 T. F. Degnan and C. R. Kennedy, *AIChE J.*, 1993, **39**, 607–614.

71 F. Alvarez, F. R. Ribeiro, G. Perot, C. Thomazeau and M. Guisnet, *J. Catal.*, 1996, **162**, 179–189.

72 J. Oenema, J. Harmel, R. Pérez Vélez, M. J. Meijerink, W.

Eijsvogel, A. Poursaeidesfahani, T. J. H. Vlugt, J. Zečević and K. P. De Jong, *ACS Catal.*, 2020, **10**, 14245–14257.

73 J. Zecevic, G. Vanbutsele, K. P. De Jong and J. A. Martens, *Nature*, 2015, **528**, 245–254.

74 G. Noh, S. I. Zones and E. Iglesia, *J. Phys. Chem. C*, 2018, **122**, 25475–25497.

75 J. Sun, C. Mu, Y. Li, Y. Zhao, S. Wang and X. Ma, *AIChE J.*, 2021, e17330.

76 K. Kaiser, M. Schmid and M. Schlummer, *Recycl. 2018, Vol. 3, Page 1*, 2017, **3**, 1.

77 D. P. Serrano, J. Aguado, J. M. Escola, J. M. Rodríguez, L. Morselli and R. Orsi, *J. Anal. Appl. Pyrolysis*, 2003, **68**–**69**, 481–494.